Acta Pharmaceutica Sinica B 2019;9(4):809–818

Chinese Pharmaceutical Association
Institute of Materia Medica, Chinese Academy of Medical Sciences

Acta Pharmaceutica Sinica B

www.elsevier.com/locate/apsb
www.sciencedirect.com

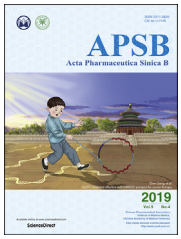

ORIGINAL ARTICLE

Novel C-17 spirost protostane-type triterpenoids from *Alisma plantago-aquatica* with anti-inflammatory activity in Caco-2 cells

Qinghao Jin[a,†], Jianqing Zhang[a,b,†], Jinjun Hou[a,†], Min Lei[a], Chen Liu[a], Xia Wang[a,c], Yong Huang[a], Shuai Yao[a], Bang Yeon Hwang[d], Wanying Wu[a,c,*], Dean Guo[a,b,*]

[a]*Shanghai Institute of Materia Medica, Chinese Academy of Sciences, Shanghai 201203, China*
[b]*School of Pharmacy, Shenyang Pharmaceutical University, Shenyang 110016, China*
[c]*University of Chinese Academy of Sciences, Beijing 100049, China*
[d]*College of Pharmacy, Chungbuk National University, Cheongju 2816, South Korea*

Received 28 February 2019; received in revised form 26 March 2019; accepted 2 April 2019

KEY WORDS

Alisma plantago-aquatica Linn.;
Protostane-type triterpenoids;
Caco-2 cells;
LPS-induced NO production

Abstract Twenty-one protostane-type triterpenoids with diverse structures, including nine new compounds (**1**–**9**), were isolated from the of *Alisma plantago-aquatica* Linn. Structurally, alisolides A–F (**1**–**6**), composed of an oxole group coupled to a five-membered ring, represent unusual C-17 spirost protostane-type triterpenoids. Alisolide H (**8**) is a novel triterpenoid with an unreported endoperoxide bridge. Alisolide I (**9**) represents the first example of 23,24-acetal triterpenoid. Their structures were elucidated based on spectroscopic analysis, wherein the absolute configurations of **4**–**6**, **8** were further confirmed by the $Mo_2(OAc)_4$-induced ECD method. Furthermore, all isolates were evaluated for their inhibitory effects on LPS-induced NO production in Caco-2 cells, and all the compounds showed remarkable inhibitory activities, with IC_{50} values in the range of 0.76–38.20 μmol/L.

*Corresponding authors.
E-mail addresses: wanyingwu@simm.ac.cn (Wanying Wu), daguo@simm.ac.cn (Dean Guo).
Peer review under responsibility of Institute of Materia Medica, Chinese Academy of Medical Sciences and Chinese Pharmaceutical Association.
[†]These authors made equal contributions to this work.

https://doi.org/10.1016/j.apsb.2019.04.002

1. Introduction

Protostane-type triterpenoids (PTs), mainly reported in plants of the genus *Alisma* Linn., are a class of natural products with fascinating and diverse carbon skeletons and intriguing biological activities. The characteristic groups of β-CH_3 in position C-10 and C-14, α-CH_3 groups in position C-8 and 21*R* configurations have made PTs hot molecules in the novel natural products discovery fields. According to our database, there are 115 bioactive PTs, such as alisols A–V[1], alismanols A–Q[2] and Alismanins A–C[3], that have been isolated from *Alisma* Linn. genus, and some of them displayed remarkable pharmacological effects, including anti-hyperlipidemic, antidiabetes, anti-tumor, anti-complement, anti-inflammatory, anti-HBV[4–9], etc. Of these, however, the majority just belongs to carbonylation derivatives of alisols A–F type PTs. Some other novel and diverse PTs have rarely been reported, such as spirost protostane-type PTs, which not only have incredibly complicated structures but also show significant biological activities in our preliminary study.

To investigate unique and biologically active natural spirost protostane-type triterpenoids from plants of the genus *Alisma* Linn., we described the investigation on systematic phytochemical profiles of 17-spirost PTs in the rhizome of *Alisma plantago-aquatica*, called "Chuan Zexie", which is widely distributed in the marshes in Sichuan province of China. However, the low concentrations of these compounds prevented us from isolating and identifying them. In this work, UPLC-Orbitrap-QDa guided isolation as well as rapid separation were performed and resulted in the isolation of nine undescribed PTs, alisolides A–I (**1**–**9**), with an spirost functionality at C-17, together with twelve known PTs, neoalisol (**10**)[10], alisol B (**11**)[11], alisol B 23 acetate (**12**)[11], alisol C 23 acetate (**13**)[11], alisol A (**14**)[12], alisol A 24 acetate (**15**)[11], 16-oxo-alisol A(**16**)[13], alisol E 23 acetate(**17**)[14], alisol F (**18**)[14], alisol F 24 acetate (**19**)[15], 11-anhydroalisol F (**20**)[16], alisol O (**21**)[17], which can be divided into nor-protostane-type PTs, carbonylation derivatives of alisol A and alisol B-type PTs, and dehydroxylation derivatives of alisol A and alisol B-type PTs (see Fig. 1). *A. plantago-aquatica* has been widely used in traditional Chinese medicine for excreting dampness and eliminating edema[1] and for the treatment of diarrhea[18]. As we all know, sometimes diarrhea is related to intestinal inflammations, hence all isolates were evaluated for their inhibitory effects on LPS-induced NO production in Caco-2 cells.

2. Results and discussion

Alisolide A (**1**), was purified as a white, amorphous powder, and its molecular formula was found to be $C_{26}H_{36}O_5$, established from HR-ESI-MS data at *m/z* 429.2617 ($[M + H]^+$, Calcd. for 429.2641), indicative of nine degrees of unsaturation. The ^1H NMR spectrum (Table 1) of **1** displayed characteristic signals attributed to six methyl protons at δ_H 1.08 (3H, s, CH_3-29), 1.11 (3H, s, CH_3-28), 1.12 (3H, s, CH_3-19), 1.17 (3H, s, CH_3-18), 1.19 (3H, d, J = 7.0 Hz, CH_3-21), 1.53 (3H, s, CH_3-30), one oxygenated methane or oxymethine at δ_H 4.11 (1H, m, H-16), and

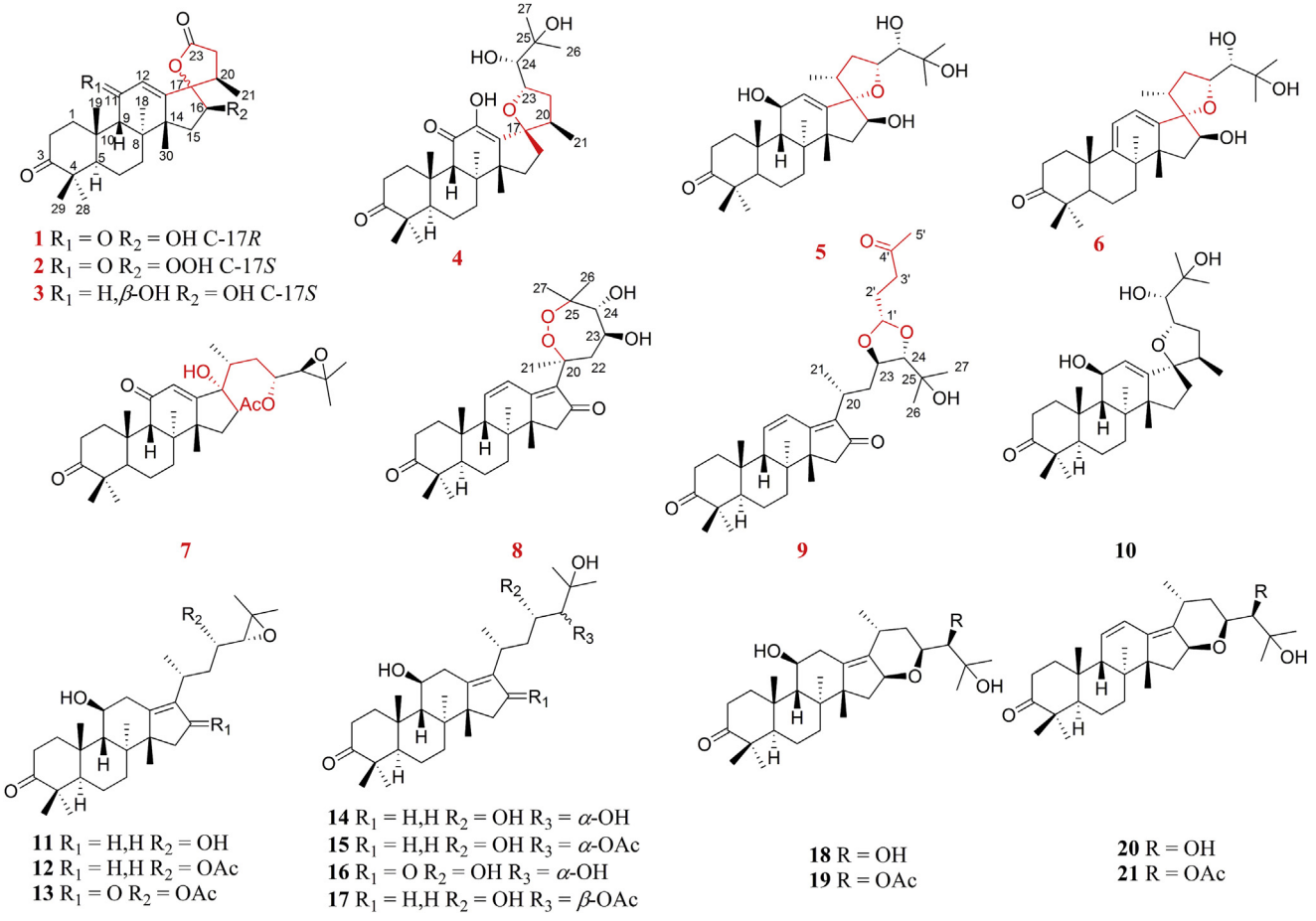

Figure 1 The structures of compounds **1**–**21**.

Table 1 ^{1}H and ^{13}C NMR data of compounds **1–3** ($CDCl_3$).

No.	1[a]		2[a]		3[b]	
	δ_H	δ_C	δ_H	δ_C	δ_H	δ_C
1	1.89, m	32.3	2.45, m; 1.88, m	32.5	2.11, m; 1.98, m	32.5
2	2.71, m (α); 2.33, m (β)	33.6	2.69, m; 2.31, m	33.9	2.66, m; 2.43, m	33.9
3		219.2		219.3		219.2
4		47.0		47.1		47.0
5	2.19, m	48.5	2.16, d, 12.0	48.8	1.98, m	49.4
6	1.32, m	20.1	1.57, m; 1.30, m	20.4	1.53, m; 1.31, m	20.4
7	2.18, m; 1.39, m	33.2	2.32, m; 1.39, m	33.3	1.99, m; 1.27, m	34.3
8		44.6		45.0		42.4
9	2.73, s	56.0	2.63, s	56.1	1.95, d, 9.0	49.0
10		37.3		37.5		36.9
11		199.4		198.6	4.32, dd, 9.0, 4.0	69.0
12	5.87, s	124.1	5.89, s	124.6	5.66, d, 4.0	124.6
13		162.4		163.7		144.1
14		49.3		47.0		46.2
15	2.37, m (α); 1.60, m (β)	40.6	2.27, m (α); 1.55, m (β)	39.0	1.35, m (α); 2.15, m (β)	38.7
16	4.11, m	73.8	4.35, m	77.9	4.14, t, 8.0	78.8
17		91.3		94.9		95.5
18	1.17, s	24.5	1.21, s	24.9	1.02, s	23.9
19	1.12, s	24.9	1.10, s	25.2	1.11, s	25.4
20	2.84, m	32.5	2.91, m	32.5	2.78, t, 7.0	32.5
21	1.19, d, 7.0	14.3	1.02, d, 7.0	18.6	1.04, d, 7.0	18.7
22	2.62, dd, 17.0, 12.0 2.69, dd, 17.0, 9.0	36.2	3.34, dd, 17.5, 8.0 2.21, d, 17.5	38.8	3.28, dd, 19.0, 8.0 2.16, d, 19.0	39.1
23		175.3		177.0		177.6
28	1.11, s	29.5	1.10, s	29.6	1.08, s	29.4
29	1.08, s	19.4	1.07, s	19.5	1.07, s	20.3
30	1.53, s	24.8	1.44, s	25.5	1.33, s	28.0

[a]In ^{1}H (600 MHz) and ^{13}C NMR (150 MHz).
[b]In ^{1}H (500 MHz) and ^{13}C NMR (125 MHz).

one olefinic proton at δ_H 5.87 (1H, s, H-12). The ^{13}C NMR spectrum (Table 1) of **1** showed 26 carbon signals, indicating the presence of six methyls, six methylenes, five methines (one oxygenated and one olefinic), nine quaternaries (three carbonyls, one olefinic), and chemical structure of **1** was similar to that of alisolide (23-*nor*-protostane)[19]. A detailed comparison of its ^{1}H and ^{13}C NMR data (Table 1) with those of alisolide, the C-16 carbon signal was shifted to δ_C 73.8 toward low field, suggesting that a free hydroxy group was attached to C-16, as confirmed by the 2D HMBC correlations (Fig. 2), including key correlations from H-16 to C-15, C-17, and C-20, as well as $^{1}H-^{1}H$ COSY correlations of H-16/H-15. Moreover, the relative configuration of **1** was determined by NOESY data (Fig. 3). The key NOESY cross-peaks of H-20/H-12, and CH_3-21/H-16 indicated that C-20 and C-17 were *R** stereochemistry.[19] The NOESY spectrum correlations were also observed between H-15α to H-16, CH_3-18; CH_3-18 to H-5, indicating that H-5, H-16, and CH_3-18 were α-orientation, and H-9β to CH_3-19, CH_3-30 indicated that CH_3-19, CH_3-30 were β-configuration (Fig. 3). Therefore, the structure of **1**, which belongs to PT with an unusual C_{17} spirost, was asserted as a 23-*nor*-protostane and named alisolide A.

Alisolide B (**2**), originally obtained as a white, amorphous powder, was designated with the molecular formula $C_{26}H_{36}O_6$ (nine degrees of unsaturation), as determined by HR-ESI-MS data at *m/z* 445.2572 ($[M + H]^+$, Calcd. for 445.2590). Based on the detailed analysis of its ^{1}H and ^{13}C NMR spectra (Table 1), the chemical structure of **2** was found to be similar as that of **1**. The difference was that substitution at C-16 location was hydroxy unit (–OH) in **1**,

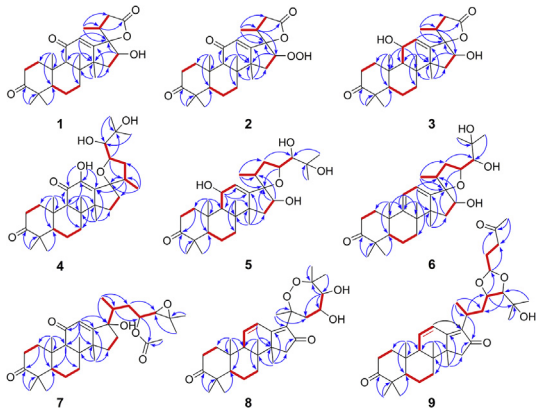

Figure 2 Selected HMBC (→) and COSY (—) correlations of compounds **1**—**9**.

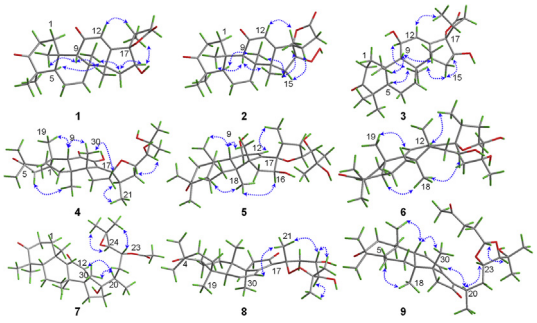

Figure 3 Selected NOESY (⟷) correlations of compounds **1**—**9**.

whereas hydroxyl peroxide unit (–OOH) in **2**. Compared with **1**, the H-16 NMR signal was shifted to low field with $\Delta\delta_H$ +0.24 in ^{1}H NMR data, and $\Delta\delta_C$ +3.6 in ^{13}C NMR data, suggesting that **2** possessed a free hydroxyl peroxide group at C-16[20], as confirmed by the tandem mass spectrometric fragmentation behaviors (ESI-MS^n) of **2**. The structures of **2** and **1** were similar, so the tandem mass spectrometric fragmentation behaviors (ESI-MS^n) of **1** and **2** were investigated by UHPLC/LTQ-Orbitrap performed in the positive mode as shown in Supporting Information Figs. S11−12 and S23−24. In the ESI-MS^3 spectra of compound **2**, we can see the cleavage of the peroxide-bridge generating an abundant ion at *m/z* 427.2743 which represents the loss of a H_2O (18 Da). And the fragmentation behaviors of compound **2** are similar to compound **1**, the difference is that there are 16 (O) units more than that of compound **1** for all corresponding fragments, which means that an carbonyl group was generated after the cleavage of the peroxide-bridge[21,22].

The planar structure of **2** was supported based on its HSQC, HMBC, and ^{1}H−^{1}H COSY data. The NOESY correlations of H-20/H-15β, and CH_3-21/CH_3-30, H-12 indicated that C-20 and C-17 were *R** and *S** configurations, respectively[19]. In the NOESY spectrum (Fig. 3), the correlations between H-15α and H-16, CH_3-18; CH_3-18 and H-5 indicated that H-5, H-16, and CH_3-18 were all α-orientation, while interactions of H-9β and CH_3-19, CH_3-30 showed that CH_3-19, CH_3-30 were β-configuration. Accordingly, the structure of **2**, which represents a previously undescribed C_{17} spirost PT, was defined and named alisolide B.

Alisolide C (**3**) was originally obtained as a white, amorphous powder and had the molecular formula $C_{26}H_{38}O_5$, according to the ^{13}C NMR and HR-ESI-MS analysis (*m/z* 431.2789, $[M + H]^+$ (Calcd. for 431.2797), which was 2 mass units more than that of compound **1**. The 1D NMR data (Table 1) of **3** showed close similarities to those of **1**, and the main difference was that chemical shift at C-11 (δ_C 69.0, δ_H 4.32, dd, 9.0, 4.0) in **3** was reduced, compared to that carbon (δ_C 199.4) in **1**. Moreover, the C-12 (δ_H 5.66, d, 4.0) in **3** was deshielded. The data indicated that a hydroxyl group was substituted in C-11. The planar structure of **3** was supported by its HSQC, HMBC, and COSY data. The same relative configuration was inferred for compounds **3** and **2** on the NOESY spectra (Fig. 3). Besides, 11-OH and 16-OH was assigned to a β position because the NOESY correlation was observed between H-11, H-16 and CH_3-18. Therefore the structure of **3** was elucidated and given a trivial name alisolide C.

Alisolide D (**4**), isolated as a white, amorphous powder, had a molecular formula of $C_{30}H_{46}O_6$, indicative of eight degrees of unsaturation, as assigned by a protonated molecular ion at *m/z* 503.3368 ($[M + H]^+$ Calcd. for 503.3373) from its HR-ESI-MS data. The ^{1}H NMR spectrum showed eight methyl signals at δ_H 0.96 (3H, d, 7.0 Hz, CH_3-21), 1.06 (3H, s, CH_3-28), 1.08 (3H, s, CH_3-19), 1.11 (3H, s, CH_3-29), 1.22 (3H, s, CH_3-26), 1.24 (3H, s, CH_3-27), 1.27 (3H, s, CH_3-18), and 1.36 (3H, s, CH_3-30). Analysis of the ^{13}C NMR and DEPT-135 NMR data of **4** revealed 30 carbon signals, which were attributed to eight methyls, seven methylenes, five methines, and ten quaternary carbons. The presence of a carbonyl carbon at δ_C 195.8 (C-11), and two olefinic carbons δ_C 140.9 (C-12), and δ_C 138.6 (C-13) accounted for two of eight degrees of unsaturation, illustrating that **4** had a α,β-unsaturated ketones in C ring. In the HMBC spectrum (Fig. 2), the key correlations of H-9 (2.84, s) with C-11, C-12, and C-14, of CH_3-30 with C-13, and C-14 further verified our conclusion. A side-by-side comparison of ^{1}H and ^{13}C NMR data of **4** with those of neoalisol (**10**)[10] indicated that **4** had a similar side chain structure with neoalisol, which was supported based on the key HMBC correlations of CH_3-21 to C-17 (δ_C 92.4), C-20 (δ_C 38.1), and C-22 (δ_C 37.8), of CH_3-26 and CH_3-27 to C-24 (δ_C 78.4), and C-23 (δ_C 77.6); and key ^{1}H−^{1}H COSY correlations of H-20 (δ_H 3.20, m) to CH_3-21, and H-22 (δ_H 2.19, m; 1.83, m), of H-23 (δ_H 4.43, br d, 9.5 Hz) to H-22, and H-24 (δ_H 3.15, br d, 10.0 Hz) (Fig. 2). Therefore, the planar structure of **4** was determined. Furthermore, in the NOESY experiment (Fig. 3), the interaction of CH_3-21 with H-16α indicated that C-17 was R^* configuration. The absolute configuration of C-24 was determined *via* $Mo_2(OAc)_4$-induced ECD method developed by Snatzke[23−26]. The positive Cotton effect at 316 nm indicated a 24 *S* configuration[27]. Thus the structure of **4** was defined and named alisolide D.

Alisolide E (**5**) was isolated as a white, amorphous powder with a molecular formula of $C_{30}H_{48}O_6$, as deduced from the HR-ESI-MS data at *m/z* 487.3416 ($[M\text{-}H_2O + H]^+$, Calcd. for 487.3423). The ^{1}H and ^{13}C NMR spectra showed characteristic signals attributed to eight methyl characteristic signals of protostane triterpenoid, and then an enol unit, three oxygenated methine groups. The structure of **5** was deduced based on the HMBC correlations (Fig. 2) from H-11 to C-9, C-10, C-12, and C-13; H-12 to C-9, C-14, and C-17; H-16 to C-13, C-14, C-15, and C-17; CH_3-21 to C-17, C-20, and C-21; H-23 to C-17, C-22, C-24; CH_3-26 and 27 to C-24, and C-25, coupled with the NOESY experiment (Fig. 3). The NOESY experiment showed correlation between CH_3-21 to H-12 indicated that C-17 spirost ring group was S^* configuration. The interaction of H-16 to CH_3-18 suggested that 16-OH was β orientation. The $Mo_2(OAc)_4$-induced ECD spectrum of **5** (Fig. 4) showed a positive Cotton effect at 313 nm, indicating a C-24 *S* configuration. The structure of **5** was therefore elucidated and given a trivial name alisolide E.

Alisolide F (**6**) was obtained as a white, amorphous powder. Its molecular formula was established as $C_{30}H_{46}O_5$ according to the HR-ESI-MS peak at *m/z* 487.3412 $[M + H]^+$ (Calcd. for 487.3423), which was 18 (H_2O) mass units less than that of compound **5**. The similarities of ^{1}H and ^{13}C NMR data of **6** and **5** suggested that these two compounds belong to 17-spirost PTs, and their structures were found to be exactly similar. The difference was that the hydroxyl group (11-OH) was dehydrated with the proton (H-9) in **5** to form a double bond ($\Delta_{9,11}$) in **6**. The plane structure of **6** was supported by its HSQC, HMBC, and COSY data. The same relative configuration was inferred for compounds **6** and **5** on the NOESY spectra (Fig. 3). The $Mo_2(OAc)_4$-induced ECD spectrum of **6** (Fig. 4) showed a positive Cotton effect at 296 nm, indicating a C-24 *S* configuration. Hence, the structure of **6** was defined and named alisolide F.

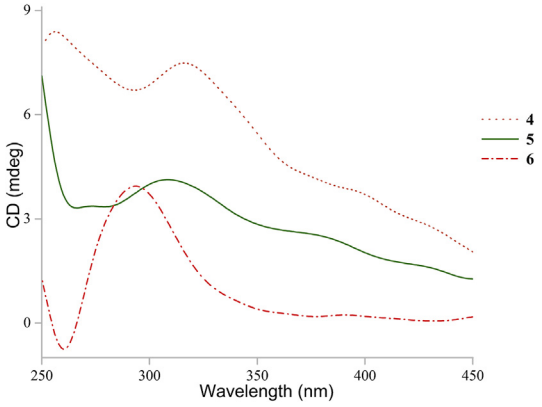

Figure 4 $Mo_2(OAc)_4$-induced ECD spectra of compounds **4**−**6**.

Alisolide G (**7**), isolated as a white, amorphous powder, showed a protonated molecular ion at *m/z* 529.3519 ($[M + H]^+$, Calcd. for 529.3529) in the HR-ESI-MS analysis, in accordance with the molecular formula $C_{32}H_{48}O_6$. Inspection of the 1D and 2D NMR spectra of **7** and alisol Q 23 acetate[28] suggested that these two compounds shared the same planar structure. An α,β-unsaturated ketones unit was also located in **7**, which was confirmed by the HMBC correlations of C-ring (H-9 to C-11, C-12, and C-14; H-12 to C-9, and C-14; CH_3-30 to C-13). A hydroxy group was present in **7**, and the position of hydroxyl group was assigned to be at C-17 based on the HMBC correlations (Fig. 2) from both CH_3-21 to C-17, and H-12 to C-17. The structure of **7** was supported by its HSQC, HMBC, and COSY data, together with the NOESY correlations. The NOESY correlations of CH_3-30 (δ_H 1.34, s) and H-20 (δ_H 2.10, m), H-20 and H-12 suggested the β configuration of C-17, and the NOSEY correlation of H-20 (δ_H 2.10, m) and H-12 (δ_H 6.16, s) revealed that C-20 was R^* configuration. In addition, the NOSEY correlations from H-24 to CH_3-27, and H-23 to CH_3-26 in combination with the characteristic NMR data of δ_H 5.25 (1H, td, J = 9.0, 4.5 Hz, H-23) and δ_H 3.03 (1H, d, J = 9.0 Hz, H-24) suggested that **7** shared the same side chain with 16β-acetoxy alisol B[24,29]. Thus, the structure of **7** was determined and named as alisolide G.

Alisolide H (**8**), isolated as a white, amorphous powder, and showed a protonated molecular ion at *m/z* 501.3208 ($[M + H]^+$, Calcd. for 501.3216) in the HR-ESI-MS analysis, corresponding to the molecular formula $C_{30}H_{44}O_6$. The ^{1}H NMR and ^{13}C NMR data of **8** showed close resemblances to the known compound 16-oxo-11-anhydroalisol A[30] with same structure of A, B, C and D rings, differing only in that of their side chains. A detailed comparison of its ^{1}H and ^{13}C NMR data with those of toonaciliatavarin C[31] and garcimultiflorone Q[32] indicated the presence of the same hydroperoxy ring substructure in **8** according to its degree of unsaturation, in which the peroxide-bearing quaternary carbon was substantially shifted to low filed compared to oxygen-bearing quaternary carbon, as confirmed by the HMBC correlations (Fig. 2) from CH_3-21 (δ_H 1.31, s) to C-17 (δ_C 139.2), C-20 (δ_C 82.4), and C-22 (δ_C 42.5); CH_3-26 (δ_H 1.37, s) and 27 (δ_H 1.19, s) to C-24 (δ_C 82.8), and 25 (δ_C 83.3). In order to confirm the peroxide-bearing substitutation, the tandem mass spectrometric fragmentation behaviors (ESI-MS^n) of **8** was investigated (Supporting Information Figs. S85 and 86). In the ESI-MS^2 spectra, we can see the cleavage of the peroxide-bridge generating an ion at *m/z* 467.3172, which represents the loss of two hydroxyl groups (34 Da)[21,22]. This hydroperoxy ring structure was rarely seen in triterpenoids. The relative configuration of **8** was deduced from the NOESY correlations and $Mo_2(OAc)_4$-induced ECD method. The key correlations between H-12 to CH_3-21; H-23 to CH_3-21, and CH_3-26; H-24 to CH_3-27, and a positive Cotton effect at 303 nm in $Mo_2(OAc)_4$-induced ECD spectrum of **8** (Fig. 5) indicated that C-23 and C-24 were *S* and *R* configuration, respectively. Thus, the structure of **8** was determined and named as alisolide H.

Alisolide I (**9**), obtained as a white, amorphous powder, and its HR-MS showed a protonated molecular ion at *m/z* 569.3840 ($[M + H]^+$, Calcd. 569.3842), corresponding to the molecular formula $C_{35}H_{52}O_6$. The NMR data were analyzed and the structures of **9** and **8** were found to be very similar, differing only in C-17 side chain. This conclusion was further supported by the HMBC spectrum (Fig. 2) of CH_3-21 (δ_H 1.20, d, 7.0) to C-17 (δ_C 138.3), C-20 (δ_C 27.6), and C-22 (δ_C 38.8); CH_3-26 (δ_H 1.17, s) and 27 (δ_H 1.04, s) to C-24 (δ_C 88.3), and 25 (δ_C 70.1); H-24 (δ_H 3.40, d, 6.0) to C-22; H-23 (δ_H 3.69, m) to C-20, C-25,

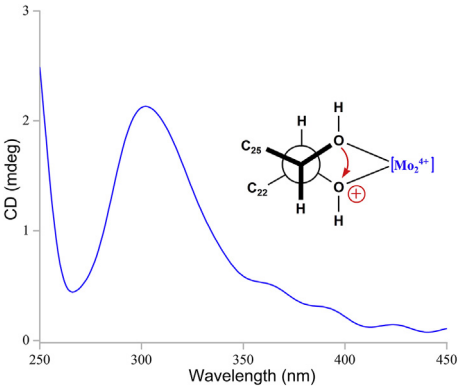

Figure 5 $Mo_2(OAc)_4$-induced ECD spectra of compound **8**.

and C-1′ (δ_C 101.5); H-1′ (δ_H 5.02, t, 4.5) to C-2′ (δ_C 27.8); CH_3-5′ (δ_H 2.15, s) to C-3′ (δ_C 37.8), and C-4′ (δ_C 208.6). The relative configuration of **9** was deduced from the NOESY correlations (Fig. 3). The doublet of H-24 (J = 6.0 Hz) observed in the ^{1}H NMR spectrum indicated the *threo* 23, 24 configuration. On the basis of the 20*R* configuration in protostane triterpenoids isolated from *Alisma. orientale* and the correlations of H-20β (δ_H 2.91, m) to H-23 and H-12 (δ_H 6.65, dd, 10.0, 3.5 Hz), H-24 to H-1′ observed in its NOESY spectrum, the 23*R** and 24*S** configurations of compound **9** were established[24,31]. Thus, the structure of **9** was defined and named alisolide I.

Chronic and acute diarrhea is strongly correlated with intestinal inflammations[33]. Considering the treatment for diarrhea of the *A. plantago-aquatica*, the aim of this study is therefore to further investigate the anti-inflammatory activities of the identified PTs of *A. plantago-aquatica*, including the six unique 17-spirost PTs, using an *in vitro* model of inflammation in Caco-2 epithelial cell lines.

The anti-inflammatory activities of the novel 17 spirost PTs (**1**−**7**) and alisolides H−I (**8**−**9**), and other PTs (**10**−**21**) were evaluated on the NO production in LPS-stimulated Caco-2 cells, and the inhibition results are shown in Table 4. All the PTs showed remarkable inhibitory activities against the NO production with IC_{50} ranging from 0.76 to 38.20 μmol/L, compared to dexamethasone, a drug currently used for the treatment of anti-inflammation. Of these, 17*R*-spirost PTs showed significant inhibitory activities, displaying an IC_{50} of 1.98−12.00 μmol/L, and, in contrast, 17-spirost *nor*-PTs existed moderate inhibitory with IC_{50} from 14.60 to 36.15 μmol/L. Alisol B 23 acetate (**12**), the major PT in *Alisma*, showed an IC_{50} value of 0.76 μmol/L.

The structure–activity relationships of the isolated compounds were illustrated in Fig. 6, in which 17*R*-spirost protostane-type PTs showed dramatic improvement in anti-inflammatory activities than 17*S* close analogues, suggesting that spatial configuration is essential to the anti-inflammatory activity. For nor-PTs (**1**−**3**), in contract, a decrease in activity was observed when the 17*R* absolute configuration changed to 17*S*, which verified the configuration issue of crucial importance. Moreover, the hydroxy group in position 11 (**3**) displayed moderate reduced anti-inflammatory activity compared to ketone replacement (**2**). In carbonylation derivatives of alisol F type PTs (**18**−**21**), there was no significant difference between alisol F (**18**) and alisol F 24 acetate (**19**) suggesting that C-24 acetate has no effect on anti-inflammatory activity, and the analogues (**20**−**21**) showed similar potent activities. Additionally, compound **20** achieved a significantly improved anti-inflammatory activity *versus* the 11-hydrogen analogue **18**, identifying that the double bond in

Table 2 ^{1}H (500 MHz) and ^{13}C (125 MHz) NMR data of compounds **4–7**.

No.	4[a]		5[a]		6[a]		7[b]	
	δ_H	δ_C	δ_H	δ_C	δ_H	δ_C	δ_H	δ_C
1	1.95, m	32.5	2.15, m	32.4	2.22, m; 1.68, m	39.6	2.66, m; 2.04, m	33.4
2	2.71, m;	33.8	2.67, m	33.9	2.80, td, 14.5, 6.0	34.8	2.81, m	34.4
	2.32, m		2.45, m		2.30, ddd, 14.5, 4.5, 3.0		2.32, m	
3		219.3		219.7		216.5		218.8
4		47.1		47.0		48.5		47.5
5	2.19, m	48.3	2.00, m	49.3	1.86, dd, 10.5, 8.5	44.9	2.30, m	48.3
6	1.48, m; 1.30, m	20.3	1.51, m; 1.32, m	20.4	1.73, m	17.5	1.48, m; 1.34, m	20.7
7	2.17, m	33.6	1.97, m	34.2	2.01, m, 1.33, m	22.8	2.27, m; 2.11, m	33.9
8		50.6		42.3		39.5		44.9
9	2.84, s	54.8	1.92, d, 9.0	49.3		153.5	2.82, s	56.2
10		37.4		36.8		38.3		38.0
11		195.8	4.30, dd, 9.0, 4.0	69.3	5.62, d, 5.0	114.4		200.6
12	6.58, s (OH)	140.9	5.58, d, 4.0	123.2	5.77, d, 5.0	118.2	6.16, s	121.8
13		138.6		147.7		144.9		177.4
14		44.8		45.3		42.1		52.7
15	1.72, m	30.9	2.06, m	37.8	2.14, dd, 14.0, 8.5	37.2	2.24, m	30.4
	1.40, m		1.19, m		1.24, dd, 14.0, 11.0		1.38, m	
16	2.08, m; 1.86, m	32.3	3.76, dd, 10.5, 9.0	80.6	4.06, dd, 11.0, 8.5	81.2	1.90, m	33.5
17		92.4		95.2		95.3		84.3
18	1.27, s	25.1	0.97, s	23.8	1.029, s	21.3	1.40, s	24.8
19	1.08, s	24.4	1.10, s	25.4	1.36, s	23.3	1.28, s	25.7
20	3.20, m	38.1	2.46, m	34.1	2.45, t, 7.0	34.4	2.10, m	35.9
21	0.96, d, 7.0	13.7	0.92, d, 7.0	18.3	0.89, d, 7.0	18.2	1.40, d, 7.0	16.1
22	2.19, m	37.8	2.66, m	36.7	2.66, m	36.5	2.05, m	36.4
	1.83, m		1.69, m		1.70, m		1.82, m	
23	4.43, br d, 9.5	77.6	4.51, dd, 10.0, 7.0	76.5	4.52, dd, 10.0, 7.0	76.5	5.25, td, 9.0, 4.5	73.5
24	3.15, br d, 10.0	78.4	3.27, br s	76.0	3.27, s	76.1	3.03, d, 9.0	65.4
25		73.4		73.4		73.4		59.5
26	1.22, s	27.0	1.25, s	27.5	1.27, s	26.9	1.30, s	25.0
27	1.24, s	26.7	1.37, s	26.8	1.38, s	27.4	1.35, s	20.3
28	1.06, s	19.4	1.07, s	20.2	1.01, s	24.5	1.12, s	29.5
29	1.11, s	29.5	1.06, s	29.3	1.15, s	21.3	1.18, s	20.1
30	1.36, s	21.8	1.26, s	27.3	1.034, s	19.6	1.34, s	22.4
24-OH	3.66, d, 10.0							
-OAc							2.07, s	21.5, 170.6

[a]In $CDCl_3$.
[b]In pyridine-d_5.

position 11 provides a significant improvement in potency. Similarly, alisol A 24 acetate (**15**) appeared in close anti-inflammatory activity (IC_{50} = 4.64 μmol/L) *versus* alisol A (**14**, IC_{50} = 2.19 μmol/L). Replacement of the 16-hydrogen with ketone (**16**) remained to achieve reduced activity for alisol A-type PTs. For alisol B-type PTs, and replacement of the 16-hydrogen with either ketone (**13**) resulted in a modest loss of anti-inflammatory activities and, in contrast, the 23-acetyl group (compound **12**) proved to be not changed compared to **11**.

3. Conclusions

To sum up, twenty-one protostane-type triterpenoids with diverse structures, including nine new ones (**1**−**9**), were isolated and identified from the rhizome of *A. plantago-aquatica* Linn. distributed in the marshes in Sichuan province of China. Structurally, alisolides A–F (**1**−**6**) represent an unprecedented C_{17} spirost protostanes-type triterpenoids with an oxole group coupled to a five-membered ring; Alisolide G (**8**) is a novel triterpenoid with a specific endoperoxide bridge; Alisolide I (**9**) represents the first example of 23,24-acetal triterpenoid. All the PTs showed remarkable inhibitory activities against the NO production with IC_{50} ranging from 0.76 to 38.20 μmol/L, and 17*R*-spirost PTs showed significant inhibitory activities, displaying an IC_{50} of 1.98−12.00 μmol/L. Compounds **11**, **12**, **20** and **21** exhibited significant inhibitory effects against NO production in Caco-2, with IC_{50} values of 0.88, 0.76, 1.17 and 1.67 μmol/L, respectively.

4. Experimental section

4.1. General experimental procedures

Optical rotation data were acquired on an Autopol VI polarimeter from Rudolph Research Analytical (Hackettstown, NJ, USA). IR data were determined on a Thermo Scientific Nicolet iS5 FT-IR spectrometer and processed using the Thermo Scientific OMNIC v9.1 software (San Jose, CA, USA). The Shimadzu UV-2450 spectrophotometer (Shimadzu, Japan) was used to measure the UV data. HR-ESI-MS data were measured on an LTQ-Orbitrap Velos Pro hybrid mass spectrometer (Thermo Fisher Scientific,

Table 3 ^{1}H (500 MHz) and ^{13}C (125 MHz) NMR data of compounds **8** and **9** ($CDCl_3$).

No.	8		9	
	δ_H	δ_C	δ_H	δ_C
1	2.12, m	32.4	2.10, m	32.4
2	2.70, m	33.4	2.74, m	33.4
	2.10, m		2.32, m	
3		219.4		219.3
4		47.3		47.3
5	2.30, m	46.2	2.33, m	46.2
6	1.60, m; 1.21, m	19.5	1.56, m; 1.17, m	19.5
7	2.15, m	31.4	2.11, m	31.4
8		48.5		48.2
9	2.37, m	47.6	2.39, m	47.9
10		36.1		36.1
11	7.30, dd, 10.5, 3.5	124.9	6.16, dd, 10.0, 2.0	122.3
12	6.15, dd, 10.5, 2.0	138.1	6.65, dd, 10.0, 3.5	138.2
13		170.5		171.7
14		40.2		39.2
15	2.36, d, 18.5	44.7	2.36, m	44.8
	1.94, d, 18.5		1.91, d, 18.5	
16		206.5		207.8
17		139.2		138.3
18	0.94, s	21.8	0.97, s	22.1
19	0.95, s	24.8	0.95, s	24.9
20		82.4	2.91, m	27.6
21	1.31, s	23.4	1.20, d, 7.0	19.6
22	2.70, m	42.5	2.02, m	38.8
	2.17, m		1.67, m	
23	3.88, t, 9.5	68.7	3.69, m	75.7
24	3.19, d, 9.0	82.8	3.40, d, 6.0	88.3
25		83.3		70.1
26	1.37, s	26.1	1.17, s	27.1
27	1.19, s	23.9	1.04, s	24.9
28	1.09, s	19.3	1.09, s	19.3
29	1.06, s	29.4	1.06, s	29.4
30	1.18, s	23.9	1.13, s	24.2
1′			5.02, t, 4.5	101.5
2′			1.97, m	27.8
3′			2.52, m	37.8
4′				208.6
5′			2.15, s	29.9

San Jose, CA, USA). NMR spectra were acquired on a Bruker Avance III HD Ascend 500 MHz spectrometer (Bruker BioSpin AG, Fällanden, Switzerland) or Bruker Avance III HD 600 MHz spectrometer (Bruker BioSpin AG, Fällanden, Switzerland) using tetramethylsilane as an internal standard, with chemical shifts (δ) expressed in ppm. All of the NMR data were reported in the paper were derived from ^{1}H NMR, ^{13}C NMR, DEPT-135 NMR, $^{1}H-^{1}H$ COSY, HSQC, HMBC, NOESY experiments. CD spectra were recorded in DMSO determined on a JASCO J-815 spectropolarimeter. Preparative HPLC was carried out on Agilent 1200 HPLC system with a PRC-ODS column (50 cm × 34 mm). Semi-preparative high-performance liquid chromatography (HPLC) separations were carried out on an Agilent 1100 liquid chromatograph with a DAD or VWD detector using a ZORBAX SB-C18 (25 cm × 9.4 mm, 5 μm; Agilent Technologies, Palo Alto, CA, USA) and Eclipse XDB-C18 column (25 cm × 9.4 mm, 5 μm; Agilent Technologies, Palo Alto, CA, USA). Column chromatography (CC) was carried out on silica gel (200−300 mesh; Qingdao Marine Chemical, Inc., Qingdao, China) and Sephadex LH-20 (GE Healthcare Bio-Sciences AB, Sweden). The UPLC−PDA-QDA analysis was performed on Waters UPLC H-Class system (Waters Corporation, Milford, MA, USA) with PDA and QDa detectors conducting on a Waters BEH C18 column (100 mm × 2.1 mm, 1.8 μm).

4.2. Plant material

The rhizome of *A. plantago-aquatica* Linn. was collected from Sichuan province, China, in December 2016 and identified by Prof. De-an Guo. A voucher specimen (Y141029) was deposited at the National Engineering Laboratory for Traditional Chinese Medicine Standardization Technology, Shanghai Institute of Materia Medica, Chinese Academy of Sciences, Shanghai, China.

4.3. Extraction and isolation

The powdered rhizome of *A. plantago-aquatica* (5.0 kg) was extracted by infusion with 100% MeOH at room temperature (24 h, 3 times). Subsequently, the residue was filtered and the solvent was evaporated under reduced pressure in a rotary evaporation equipment (Buchi, Switzerland) at a temperature of 40 °C. And then the obtained extract (573.2 g) was dissolved in distilled H_2O and

Table 4 Effects of compounds **1**–**21** on NO production in LPS-stimulated Caco-2 cells.

Compd.	IC_{50} (μmol/L)	Compd.	IC_{50} (μmol/L)	Compd.	IC_{50} (μmol/L)
1	36.15	**8**	11.48	**15**	4.64
2	14.60	**9**	12.00	**16**	34.69
3	26.93	**10**	4.43	**17**	23.49
4	1.98	**11**	0.88	**18**	27.15
5	38.20	**12**	0.76	**19**	21.86
6	20.56	**13**	12.91	**20**	1.17
7	11.20	**14**	2.19	**21**	1.67

Positive control: dexamethasone (0.5 μmol/L, inhibition rate 75.26%).

successively partitioned with *n*-hexane, CH_2Cl_2, EtOAc, and BuOH. The CH_2Cl_2 portion (142.5 g) was purified on a silica gel column (1.5 kg) to give thirty-five fractions, Fr1–Fr35, through gradient elution with changing ratios of *n*-hexane:EtOAc from 100:0 to 0:100.

Fraction 9 (3.5 g) was loaded onto RP-C18 column on MHPLC system with a gradient system of CH_3CN–H_2O (15:85–40:60, *v/v*) to obtain 10 fractions (F9a–F9i) and three compounds, **14** (15.0 mg), **11** (20.2 mg) and **13** (10.5 mg). Fraction 9i (55.0 mg) afforded **7** (2.5 mg) after semipreparative HPLC eluted with a gradient of MeOH–acetonitrile–H_2O (75:10:15, *v/v*) on an Eclipse XDB-C18 column. Fraction 10 (4.1 g) was applied to RP-C18 column with CH_3CN–H_2O (stepwise 20:80–40:60, *v/v*) as mobile phase to obtain

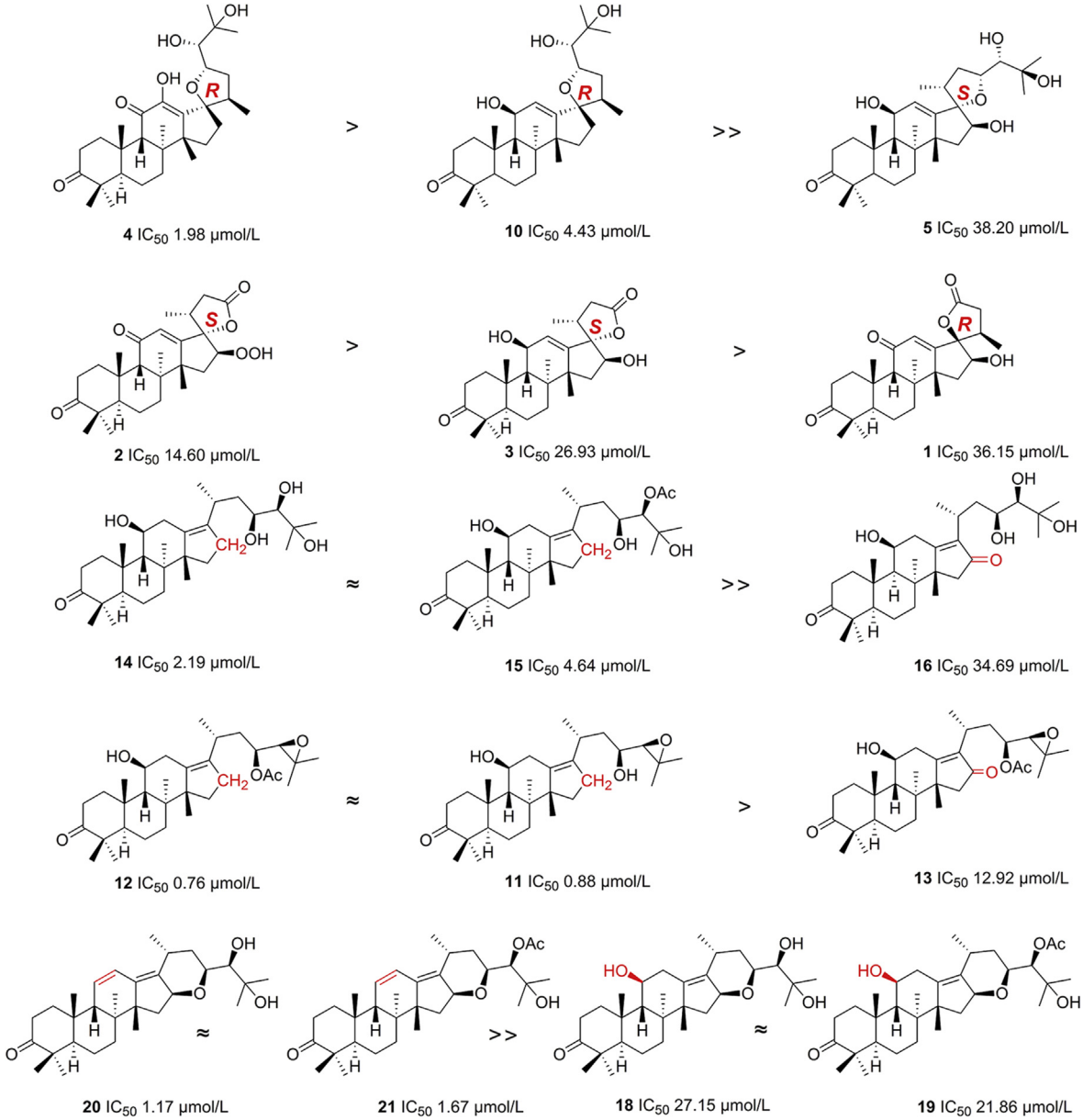

Figure 6 Structure–activity relationships of isolated compounds.

four fractions (F10a–F10d), and F10c further purified by semi-preparative HPLC (MeOH−H_2O, 85:15, 3.0 mL/min) to give compounds **1** (1.9 mg) and F10d was separated over a ZORBAX SB-C18 column (MeOH−H_2O, 80:20, 3.0 mL/min) to yield **20** (3.5 mg) and **21** (4.0 mg). Fraction 12 (4.5 g), collected in the radio of *n*-hexane:EtOAc at 1:1 of the gradient elution, was purified by preparative HPLC with a gradient elution (CH_3CN−H_2O, 15:85−80:20, 25.0 mL/min) to yield compound **18** (15.0 mg) and eight fractions (F12a–F12h). The fraction 12c (80.0 mg) was separated on a semi-preparative HPLC using an Eclipse XDB-C18 column (20% CH_3CN:80% H_2O to 100% CH_3CN:0% H_2O), giving **2** (1.8 mg) and in the same condition, compound **3** (1.1 mg) was obtained from F12d. Semipreparative HPLC of Fr12e (55.0 mg) on an Eclipse XDB-C18 column yielded **19** (8.0 mg). Further purification of Fr12f and Fr12g by semipreparative HPLC separately on an Eclipse XDB-C18 column (CH_3CN−H_2O, 70:30) and an SB-C18 column (CH_3CN−H_2O, 85:15) afforded **8** (2.3 mg) and **9** (2.6 mg). Fr12h (400 mg) was separated on an Eclipse XDB-C18 column (CH_3CN−H_2O, 70:30−100:0), giving **6** (2.3 mg). Fraction F13 was repeatedly purified by silica gel CC (Hexane–EA, from 20:1 to 50:50), preparative HPLC (CH_3CN−H_2O, 10:90−100:0, 10.0 mL/min) and semi-preparative HPLC (CH_3CN−H_2O, 70:30−100:0, 3.0 mL/min) to give compounds **4** (2.0 mg), **10** (3.5 mg) and **12** (200 mg). The fraction F14 was separated on Sephadex LH-20 (500 mm × 30 mm, 50 g) eluted with MeOH−Cl_2Cl_2 (1:1) to afford three main fractions F14a−c and F14a was further fractionated *via* RP-C18 column chromatography eluted with a step gradient of CH_3CN−H_2O (from 10:90−30:70, 25.0 mL/min) to obtain three fractions (F14a1–3). Fraction F14a2 (70.2 mg) was separated over a ZORBAX SB-C18 column (CH_3CN−H_2O, 50:50−80:20, 3.0 mL/min) to yield compound **15** (5.1 mg) and **17** (3.5 mg). Fraction F14a3 (82.2 mg) was purified by semipreparative HPLC on an Eclipse XDB-C18 column, developed with acetonitrile–H_2O (30:70−100:0, *v/v*) to give compound **5** (2.8 mg) and **16** (3.2 mg).

4.3.1. *Alisolide A (**1**)*

White, amorphous powder; UV (MeOH) λ_{max} (logε): 203.8 (4.0), 242.6 (4.2); IR (KBr) ν_{max}: 3431, 2973, 2947, 2872, 1780, 1694, 1664, 1456, 1372, 1176 cm^{-1}; HR-ESI-MS (positive) at *m/z* 429.2617 $[M + H]^+$ (Calcd. for $C_{26}H_{36}O_5$ 429.2641); ^1H (600 MHz, $CDCl_3$) and ^{13}C NMR (150 MHz, $CDCl_3$) data see Table 1.

4.3.2. *Alisolide B (**2**)*

White, amorphous powder; UV (MeOH) λ_{max} (logε): 203.6 (3.9), 241.6 (4.0); IR (KBr) ν_{max}: 3437, 2973, 2925, 2878, 1771, 1700, 1670, 1376 cm^{-1}; HR-ESI-MS (positive) at *m/z* 445.2572 $[M + H]^+$ (Calcd. for $C_{26}H_{37}O_6$ 445.2590); ^1H (600 MHz, $CDCl_3$) and ^{13}C NMR (150 MHz, $CDCl_3$) data see Table 1.

4.3.3. *Alisolide C (**3**)*

White, amorphous powder; UV (MeOH) λ_{max} (logε): 202.0 (4.1), 248.0 (3.5); IR (KBr) ν_{max}: 3432, 2962, 2941, 2878, 1742, 1691, 1465, 1382, 1260 cm^{-1}; HR-ESI-MS (positive) at *m/z* 431.2789 $[M + H]^+$ (Calcd. for $C_{26}H_{39}O_5$ 431.2797); ^1H (500 MHz, $CDCl_3$) and ^{13}C NMR (125 MHz, $CDCl_3$) data see Table 1.

4.3.4. *Alisolide D (**4**)*

White, amorphous powder; $[\alpha]_D^{20}$+ 5.8 (*c* 0.1, MeOH); UV (MeOH) λ_{max} (logε): 201.6 (4.0), 284.4 (4.0); IR (KBr) ν_{max}: 3452, 2970, 2929, 2869, 1700, 1646, 1462, 1376 cm^{-1}; HR-ESI-MS (positive) at *m/z* 503.3368 $[M + H]^+$ (Calcd. for $C_{30}H_{47}O_6$ 503.3373); $Mo_2(OAc)_4$-induced ECD (DMSO) 316 ($\Delta\varepsilon$ 7.48) nm; ^1H (500 MHz, $CDCl_3$) and ^{13}C NMR (125 MHz, $CDCl_3$) data see Table 2.

4.3.5. *Alisolide E (**5**)*

White, amorphous powder; $[\alpha]_D^{20}$+ 53.8 (*c* 0.1, MeOH); UV (MeOH) λ_{max} (logε): 204.0 (4.0), 244.4 (3.8); IR (KBr) ν_{max}: 3426, 2967, 2938, 2869, 1697, 1465, 1378 cm^{-1}; HR-ESI-MS (positive) at *m/z* 487.3416 $[M\text{-}H_2O + H]^+$ (Calcd. for $C_{30}H_{47}O_5$ 487.3423); $Mo_2(OAc)_4$-induced ECD (DMSO) 313 ($\Delta\varepsilon$ 4.09) nm; ^1H (500 MHz, $CDCl_3$) and ^{13}C NMR (125 MHz, $CDCl_3$) data see Table 2.

4.3.6. *Alisolide F (**6**)*

White, amorphous powder; $[\alpha]_D^{20}$+ 8.0 (*c* 0.05, MeOH); UV (MeOH) λ_{max} (logε): 202.0 (4.0), 274.0 (3.9); IR (KBr) ν_{max}: 3435, 2962, 2925, 2866, 1738, 1447, 1372 cm^{-1}; HR-ESI-MS (positive) at *m/z* 487.3412 $[M + H]^+$ (Calcd. for $C_{30}H_{47}O_5$ 487.3423); $Mo_2(OAc)_4$-induced ECD (DMSO) 296 ($\Delta\varepsilon$ 3.90) nm; ^1H (500 MHz, $CDCl_3$) and ^{13}C NMR (125 MHz, $CDCl_3$) data see Table 2.

4.3.7. *Alisolide G (**7**)*

White, amorphous powder; $[\alpha]_D^{20}$+ 130.0 (*c* 0.05, MeOH); UV (MeOH) λ_{max} (logε): 202.0 (4.2), 248.6 (4.4); IR (KBr) ν_{max}: 3461, 2965, 2934, 2875, 1733, 1697, 1649, 1453, 1370, 1235 cm^{-1}; HR-ESI-MS (positive) at *m/z* 529.3519 $[M + H]^+$ (Calcd. for $C_{32}H_{49}O_6$ 529.3529); ^1H (500 MHz, pyridine-d_5) and ^{13}C NMR (125 MHz, pyridine-d_5) data see Table 2.

4.3.8. *Alisolide H (**8**)*

White, amorphous powder; $[\alpha]_D^{20}$+ 148.2 (*c* 0.1, MeOH); UV (MeOH) λ_{max} (logε): 201.8 (3.9), 286.2 (4.3); IR (KBr) ν_{max}: 3444, 2970, 2866, 1697, 1602, 1453, 1376, 1233 cm^{-1}; HR-ESI-MS (positive) at *m/z* 501.3208 $[M + H]^+$ (Calcd. for $C_{30}H_{45}O_6$ 501.3216); $Mo_2(OAc)_4$-induced ECD (DMSO) 303 ($\Delta\varepsilon$ 2.13) nm; ^1H (500 MHz, $CDCl_3$) and ^{13}C NMR (125 MHz, $CDCl_3$) data see Table 3.

4.3.9. *Alisolide I (**9**)*

White, amorphous powder; $[\alpha]_D^{20}$+ 32.0 (*c* 0.1, MeOH); UV (MeOH) λ_{max} (logε): 201.8 (4.0), 285.8 (4.2); IR (KBr) ν_{max}: 3449, 2956, 2932, 2869, 1706, 1682, 1616, 1450, 1369, 1239 cm^{-1}; HR-ESI-MS (positive) at *m/z* 569.3840 $[M + H]^+$ (Calcd. for $C_{35}H_{53}O_6$ 569.3842); ^1H (500 MHz, $CDCl_3$) and ^{13}C NMR (125 MHz, $CDCl_3$) data see Table 3.

4.4. *Measurement of LPS-induced NO production on Caco-2 cells*

Caco-2 Cells, purchased from cell bank of the Chinese Academy of Sciences (Shanghai, China), were maintained in Dulbecco's modified eagle's medium (DMEM) with 20% fetal bovine serum (FBS, ThermoFisher, Cat. No. 10099-141) and 1% streptomycin/penicillin (ThermoFisher, Cat. No. 15140148). The Caco-2 cells were seeded into a 96-well microstate plate at a density of 2×10^6 cells per well and allowed 24 h to adhere before introducing Lipopolysaccharides (1 μg/mL), and then co-incubated with or without increasing the concentrations of the isolates for 24 h at 37 °C. After treatment, the Nitric Oxide concentration in the medium was measured with Nitric Oxide Assay Kit (Nanjing Jiancheng Bioengineering Institute, Nanjing, China) based on the nitrate reductase method. Absorbance was measured at 550 nm

against a calibration curve with sodium nitrite standards. The nitric oxide concentration of the wells with cells was subtracted from the nitric oxide concentration of the blank wells without cells to calculate the nitric oxide production. Cell viability of the remaining cells was determined by an MTT (Sigma Chemical Co., St. Louis, MO, USA)-based colorimetric assay[34,35].

Acknowledgments

The financial support from the National Standardization of Traditional Chinese Medicine Project (ZYBZH-C-SH-49, China), the National Natural Science Foundation of China (No. 81530095), National Standardization Program for Chinese Medicine (ZYBZH-K-LN-01, China) and Shanghai Committee of Science and Technology (16DZ0500800, China) are gratefully acknowledged. Thank Wu Jia for providing samples and helping with separation process.

Appendix A. Supporting information

Supporting data to this article can be found online at https://doi.org/10.1016/j.apsb.2019.04.002.

References

1. Tian T, Chen H, Zhao YY. Traditional uses, phytochemistry, pharmacology, toxicology and quality control of *Alisma orientale* (Sam.) Juzep: a review. *J Ethnopharmacol* 2014;**158**:373–87.
2. Zhang LL, Xu W, Xu YL, Chen XP, Huang MQ, Lu JJ. Therapeutic potential of rhizoma alismatis: a review on ethnomedicinal application, phytochemistry, pharmacology, and toxicology. *Ann N Y Acad Sci* 2017;**1401**:90–101.
3. Wang C, Huo XK, Luan ZL, Cao F, Tian XG, Zhao XY, et al. Alismanin A, a triterpenoid with a C_{34} skeleton from *Alisma orientale* as a natural agonist of human pregnane X receptor. *Org Lett* 2017;**19**:5645–8.
4. Imai Y, Matsumura H, Aramaki Y. Hypocholesterolemic effect of alisol A-24-monoacetate and its related compounds in rats. *Jpn J Pharmacol* 1970;**20**:222–8.
5. Lin HR. Triterpenes from *Alisma orientalis* act as farnesoid X receptor agonists. *Bioorg Med Chem Lett* 2012;**22**:4787–92.
6. Law BYK, Wang M, Ma DL, Al-Mousa F, Michelangeli F, Cheng SH, et al. Alisol B, a novel inhibitor of the sarcoplasmic/endoplasmic reticulum Ca^{2+} ATPase pump, induces autophagy, endoplasmic reticulum stress, and apoptosis. *Mol Cancer Ther* 2010;**9**:718–30.
7. Lee SM, Kim JH, Zhang Y, An RB, Min BS, Joung H, et al. Anti-complementary activity of protostane-type triterpenes from Alismatis Rhizoma. *Arch Pharm Res* 2003;**26**:463–5.
8. Murata T, Shinohara M, Miyamoto M. Biological-active triterpenes of Alismatis Rhizoma. IV. Structures of alisol B, alisol B monoacetate and alisol C monoacetate. Reactions of the α-hydroxy epoxide of the alisol B derivatives. *Chem Pharm Bull* 1970;**18**:1369–84.
9. Jiang ZY, Zhang XM, Zhou J, Zhang FX, Chen JJ, Lü Y, et al. Two new sesquiterpenes from *Alisma orientalis*. *Chem Pharm Bull* 2007;**55**:905–7.
10. Peng GP, Zhu GY, Lou FC. Two novel terpenoids from *Alisma orientalis* Juzep. *Nat Prod Res Dev* 2002;**14**:5–8.
11. Lee S, Kho Y, Min B, KimJ, Na M, Kang S. Cytotoxic triterpenoides from Alismatis Rhizoma. *Arch Pharm Res* 2001;**24**:524–6.
12. Murata T, Miyamoto M. Biological-active triterpenes of Alismatis Rhizoma. II. The structures of alisol A and alisol A monoacetate. *Chem Pharm Bull* 1970;**18**:1354–61.
13. Nakajima Y, Satoh Y, Katsumata M, Tsujiyama K, Ida Y, Shoji J. Terpenoids of *Alisma orientale* rhizome and the crude drug Alismatis Rhizoma. *Phytochemistry* 1994;**36**:119–27.
14. Yoshikawa M, Hatakeyama S, Tanaka N, Fukuda Y, Yamahara J, Murakami N. Crude drugs from aquatic plants. I. On the constituents of Alismatis Rhizoma. (1). Absolute stereostructures of alisols E 23-acetate, F, and G, three new protostane-type triterpenes from Chinese Alismatis Rhizoma. *Chem Pharm Bull* 1993;**41**:1948–54.
15. Peng GP, Lou FC. Terpenoids of *Alisma orientalis* Juzep. *Nat Prod Res Dev* 2001;**13**:1–3.
16. Hu XY, Guo YQ, Gao WY, Zhang TJ, Chen HX. Two new triterpenes from the rhizomes of *Alisma orientalis*. *J Asian Nat Prod Res* 2008;**10**:481–4.
17. Jiang ZY, Zhang XM, Zhang FX, Liu N, Zhao F, Zhou J, et al. A new triterpene and anti-hepatitis B virus active compounds from *Alisma orientalis*. *Planta Med* 2006;**72**:951–4.
18. Han CW, Kwun MJ, Kim KH, Choi JY, Oh SR, Ahn KS, et al. Ethanol extract of Alismatis Rhizoma reduces acute lung inflammation by suppressing NF-κB and activating *Nrf2*. *J Ethnopharmacol* 2013;**146**:402–10.
19. Zhao M, Xu LJ, Che CT. Alisolide, alisols O and P from the rhizome of *Alisma orientale*. *Phytochemistry* 2008;**69**:527–32.
20. Yamada K, Ogata N, Ryu K, Miyamoto T, Komori T, Higuchi R. Bioactive terpenoids from octocorallia. 3. A new eunicellin-based diterpenoid from the soft coral *Cladiella sphaeroides*. *J Nat Prod* 1997;**60**:393–6.
21. Fales HM, Sokolosk EA, Pannell LK, Pu L, Klayman DL, Lin AJ, et al. Comparison of mass spectral techniques using organic peroxides related to artemisinin. *Anal Chem* 1990;**62**:2494–501.
22. Fraser RTM, Paul NC, Phillips L. Mass spectrometry of some alkyl peroxides. *J Chem Soc B* 1970:1278–80.
23. Di Bari L, Pescitelli G, Pratelli C, Pini D, Salvadori P. Determination of absolute configuration of acyclic 1,2-diols with $Mo_2(OAc)_4$. 1. Snatzke's method revisited. *J Org Chem* 2001;**66**:4819–25.
24. Mai ZP, Zhou K, Ge GB, Wang C, Huo XK, Dong PP, et al. Protostane triterpenoids from the rhizome of *Alisma orientale* exhibit inhibitory effects on human carboxylesterase 2. *J Nat Prod* 2015;**78**:2372–80.
25. Frelek J, Ikekawa N, Takatsuto S, Snatzke G. Application of $[Mo_2(OAc)_4]$ for determination of absolute configuration of brassinosteroid vic-diols by circular dichroism. *Chirality* 1997;**9**:578–82.
26. Zhao JX, Liu CP, Zhang MM, Li J, Yue JM. Dysohonin A, a meroditerpenoid incorporating a 6,15,6-fused heterotricyclic ring system from *Dysoxylum hongkongense*. *Org Chem Front* 2018;**5**:2202–7.
27. Politi M, de Tommasi N, Pescitelli G, Di Bari L, Morelli I, Braca A. Structure and absolute configuration of new diterpenes from *Lavandula multifida*. *J Nat Prod* 2002;**65**:1742–5.
28. Jin HG, Jin Q, Kim AR, Choi H, Lee JH, Kim YS, et al. A new triterpenoid from *Alisma orientale* and their antibacterial effect. *Arch Pharm Res* 2012;**35**:1919–26.
29. Cang J, Wang C, Huo XK, Tian XG, Sun CP, Deng S, et al. Sesquiterpenes and triterpenoids from the rhizomes of *Alisma orientalis* and their pancreatic lipase inhibitory activities. *Phytochem Lett* 2017;**19**:83–8.
30. Tadahiro K, Masako T, Miho T, Hiroyuki I, Toshifumi H, Johji Y. Inhibitory effects and active constituents of *Alisma* rhizomes on vascular contraction induced by high concentration of KCl. *Bull Chem Soc Jpn* 1994;**67**:1394–8.
31. Zhang F, Wang JS, Gu YC, Kong LY. Cytotoxic and anti-inflammatory triterpenoids from *Toona ciliata*. *J Nat Prod* 2012;**75**:538–46.
32. Wang ZQ, Li XY, Hu DB, Long CL. Cytotoxic garcimultiflorones K–Q, lavandulyl benzophenones from *Garcinia multiflora* branches. *Phytochemistry* 2018;**152**:82–90.
33. Aranda-Michel J, Giannella RA. Acute diarrhea: a practical review. *Am J Med* 1999;**106**:670–6.
34. Lee JW, Lee C, Jin Q, Jang H, Lee D, Lee HJ, et al. Diterpenoids from the roots of *Euphorbia fischeriana* with inhibitory effects on nitric oxide production. *J Nat Prod* 2016;**79**:126–31.
35. Lee C, Lee JW, Jin Q, Lee SJ, Lee D, Lee MK, et al. Anti-inflammatory constituents from the fruits of *Vitex rotundifolia*. *Bioorg Med Chem Lett* 2013;**23**:6010–4.